06

Mechanical properties of silicified graphite at high deformation velocity

© A.M. Kuzmin,[1] A.Yu. Konstantinov,[2] G.G. Savenkov[3]

[1]JSC „Central Design Bureau of Machine Building“,
190020 St. Petersburg, Russia
[2]Lobachevsky University of Nizhny Novgorod,
603600 Nizhny Novgorod, Russia
[3]St. Petersburg State Technological Institute (Technical University),
190013 St. Petersburg, Russia
e-mail: sav-georgij@yandex.ru

Received June 6, 2024
Revised July 31, 2024
Accepted August 16, 2024

The paper presents the results of experimental studies on a split Hopkinson rod to determine the mechanical properties of SG–P 0.5P grade silicified graphite used in friction units under shock loading. It is established that dynamic indicators of strength and fracture are more than two to four times higher than similar characteristics obtained under quasi-static loading.

Keywords:split Hopkinson rod, silicified graphite, Brazilian test.

DOI: 10.61011/TP.2024.10.59361.201-24

Introduction

Carbon-silicon carbide materials are currently used in nuclear and marine engineering for certain heavy loaded parts (e.g., friction pairs in axial radial bearings and end seals, hydrocyclone nozzles, etc.). This is attributable to their unique physical, chemical, and mechanical properties, which include high oxidation resistance, the capacity to operate in aggressive environments, and high strength. Silicified graphite (SG), which is a composite material consisting of graphite, silicon carbide of exceptionally high hardness, and residual silicon ($Si+SiO_2$), is a typical material of this kind. The high-temperature strength and heat resistance of SG come from silicon carbide, and graphite lends it high thermal-cycling stability [1,2]. SG is produced by reactive impregnation of a special porous carbon base with molten silicon (or its vapors) at a temperature of 1600°C [3]. Silicon carbide forms in the process of interaction of carbon and silicon as liquid silicon spreads over the surface of the carbon base, converting 20–70% of graphite into SiC [4].

Certain parts made of SG may be subject to shock loads, which necessitates meticulous calculation studies and experimental testing. The mechanical characteristics of SG within the range of deformation rates typical of operational shock loads are needed in this case; however, such data are lacking completely in current literature. The present study is the first attempt at obtaining experimental data on the dynamic strength of SG at deformation rates $\dot{\varepsilon} < 10^4\ s^{-1}$.

1. Material and research techniques

SG-P 0.5 P silicified graphite produced in accordance with TU100−84−0001 TU 27 was chosen for tests. The composition and the physical and mechanical characteristics of SG-P 0.5 P are presented in Table 1.

An indirect (splitting) method for the determination of tensile strength (the so-called „Brazilian test“ with tensile stresses established in the center of a specimen) was used to plot the loading diagrams for SG-P. This method is applied to non-metallic brittle materials (specifically, carbon masses and graphitized products [5]). It has been proposed for static tests in 1947 by Brazilian engineer F. Carneiro (and has also been developed independently in Japan) [6]. The method has later been modified to accommodate dynamic loading with a split-Hopkinson pressure bar (SHPB) [7,8]. Experiments were performed using an SHPB-20 setup (Fig. 1) [8]

Table 1. Composition and physical and mechanical characteristics of SG-P 0.5 P

No.	Parameter	Value
1	Composition, % mass.	C: 32.6; SiC: (52.2); Si: (15.2)
2	Density, g/cm^3	2.6
3	Total porosity, %	39
4	Ultimate strength, MPa compressive tensile	 235−430 39.2
5	Young's modulus, GPa	95−160
6	Impact toughness, kJ/m^2	2.35−4.4
7	Hardness, HRB	114−125

Note. The data in rows 1−3 correspond to the tested specimens, while the data in rows 4−7 were taken from TU100−84−0001 TU 27.

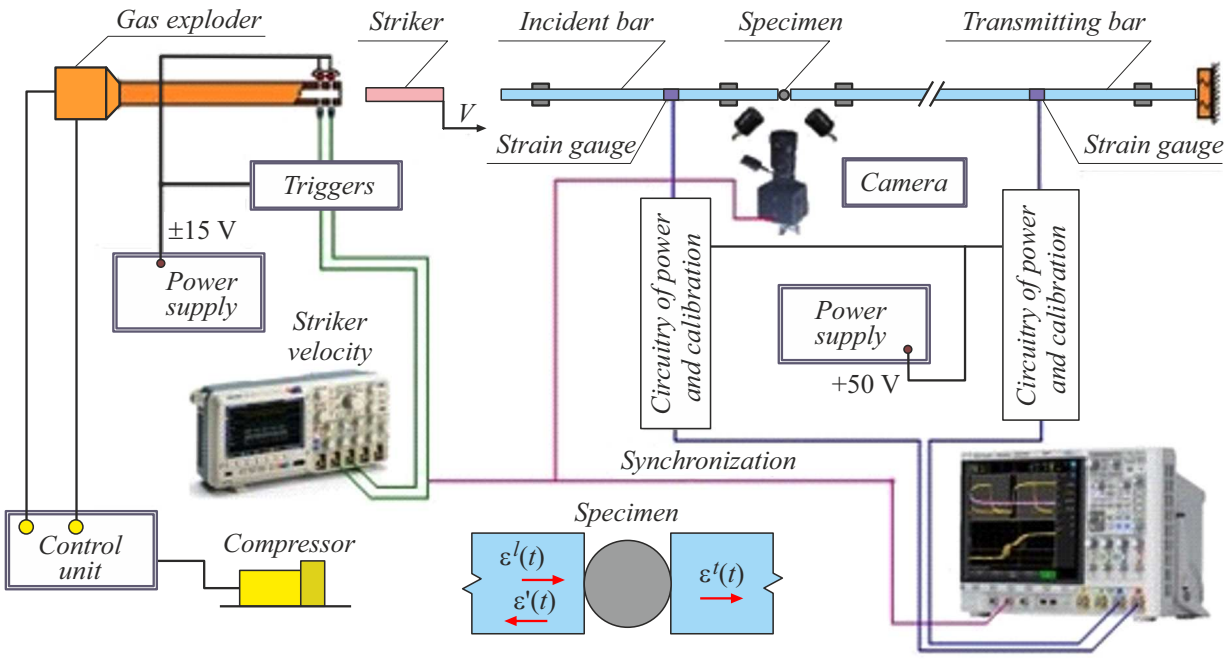

Figure 1. Schematic diagram of the experimental setup for dynamic testing.

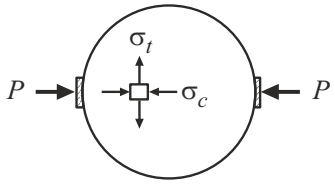

Figure 2. Stress diagram in splitting of a specimen.

with a split-Hopkinson pressure bar. The stress diagram in splitting of a specimen is shown in Fig. 2. The specimen was a disk 20 mm in diameter and 10 mm in thickness.

Incident and transmission bars, which were made of high-strength steel with a yield strength of ~ 2000 MPa, had one and the same length of 1.5 m, and the striker length was 300 mm.

The algorithm allowing one to determine compressive σ_c and tensile σ_t elastic stresses based on pulse $\varepsilon^T(t)$ transmitted through the specimen into the transmission bar is as follows. The expressions for compressive and tensile stresses obtained by solving the Hertz contact problem in the elastic formulation have the following form [6]:

$$\sigma_t = \frac{2P}{\pi HD},$$

$$\sigma_c = \frac{2P}{\pi HD} \cdot \frac{D^2}{r(D-r)},$$

where H is the thickness of the disk, D is its diameter, and r is the current coordinate along the specimen radius.

Contact force P is given by

$$P = E_b S_b \varepsilon^T(t),$$

where E_b is the Young's modulus of the bar material and S_b is the cross-section area of the measurement bar.

The velocity of impact with the incident bar was varied from ~ 9.5 to ~ 20 m/s. The tests were performed at room temperature (20°C).

The process of specimen destruction was recorded with a video camera at a rate of 140 000 frames per second.

In addition to the Brazilian splitting test, dynamic compression tests were carried out for SG P 0.5P specimens. These specimens had the shape of disks (pellets) with a diameter of 12 mm and height of 6 mm.

2. Experimental results and discussion

2.1. Experiments on splitting of specimens

Example time dependences of tensile stresses in the specimen loading plane are shown in Fig. 3. The results of experiments are presented in Table 2 and Fig. 4. The frames in Figs. 5 and 6 illustrate (left to right, top to bottom) the process of specimen destruction recorded by the high-speed video camera. Since a large number of frames were captured, only select ones are presented in these figures.

A comparison of the test results (Table 2) with the data from Table 1 reveals that the static ultimate tensile strength is more than 3–4 times lower than the dynamic ultimate strength (the maximum tensile stress withstood by a specimen under shock loading).

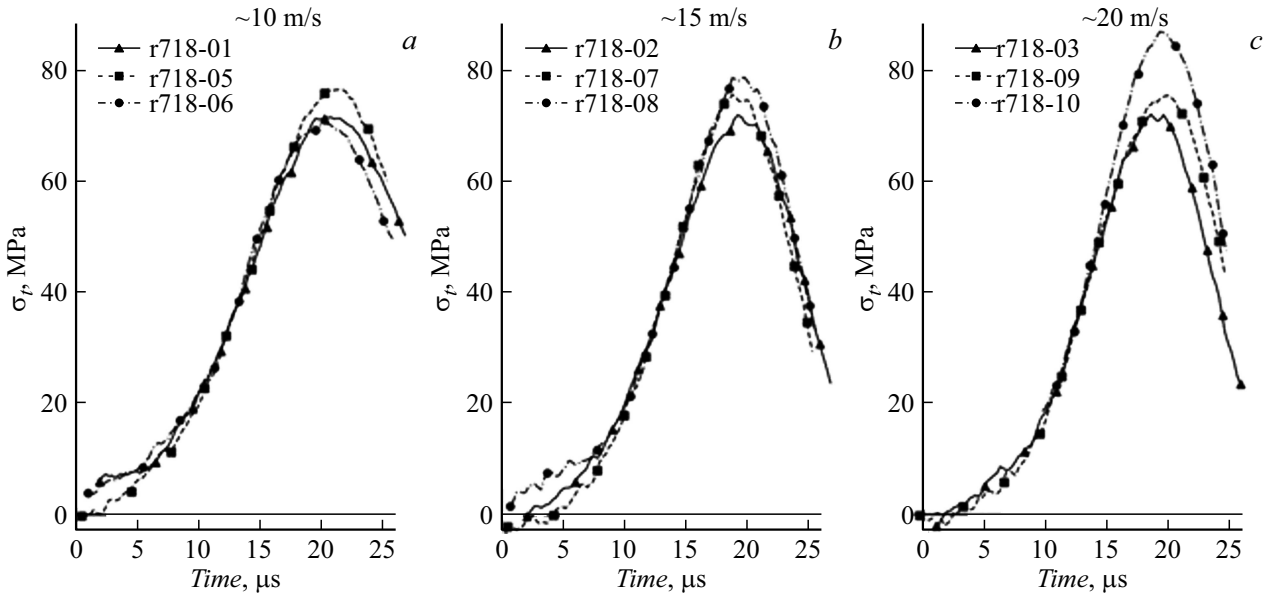

Figure 3. Specimen loading diagrams.

Table 2. Results of dynamic splitting tests

Test code	Striker velocity, m/s	Maximum tensile stresses (MTSs), MPa
r718-01	9.37	71.0
r718-05	9.45	76.0
r718-06	9.57	69.9
Average values	9.46 ± 0.1	72.3 ± 3.25
r718-02	15.76	71.4
r718-07	15.98	75.1
r718-08	15.62	78.2
Average values	15.79 ± 0.18	74.9 ± 3.56
r718-03	20.69	71.5
r718-09	20.19	74.8
r718-10	20.12	86.3
Average values	20.33 ± 0.31	77.5 ± 7.26

Note. Average values and standard deviations are presented.

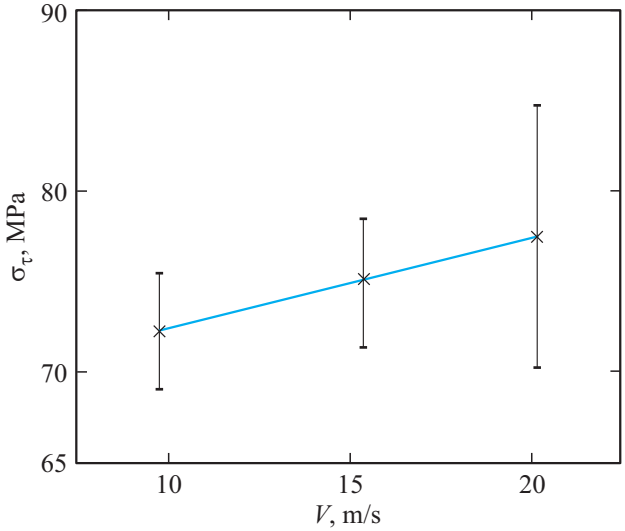

Figure 4. Dependence of MTSs on the impact velocity.

The dependence of the maximum tensile stress on the impact velocity is virtually linear within the examined velocity range (Fig. 4).

The presented frames show that a single central crack forms in the specimen at an impact velocity of 9.37 m/s. The process of crack branching is initiated almost immediately at one of its ends (Fig. 5). Although there is no known unambiguous explanation for this process, the majority of researchers believe that branching starts when the crack velocity reaches a certain (sufficiently high) critical value [9-11]. For example, the experimental results reported in [12] suggest that the deviation from rectilinear crack propagation occurs at a crack velocity of $V_c \approx 0.4c_R$ (c_R is the Rayleigh wave velocity). Therefore, an estimate of the crack velocity in the present case will be obtained below.

Since a similar isolated crack emerges at an impact velocity of $\sim$ 16 m/s, the sequence of frames corresponding to this velocity is not shown. In contrast, a system of two large cracks forms in the specimen at an impact velocity of 20.69 m/s; in addition, the regions of severe deformation (dark areas denoted by arrows) at the impacted surface are significantly larger than those observed at a velocity of 9.37 m/s.

Video recording of the process of specimen destruction provides an opportunity to estimate the SG crack velocity under dynamic loading conditions. A crack along the diameter of the specimen is seen in Fig. 5, *b*; i.e., its length is approximately equal to 20 mm (this is likely to be a slightly underestimated value). Since the time interval between two

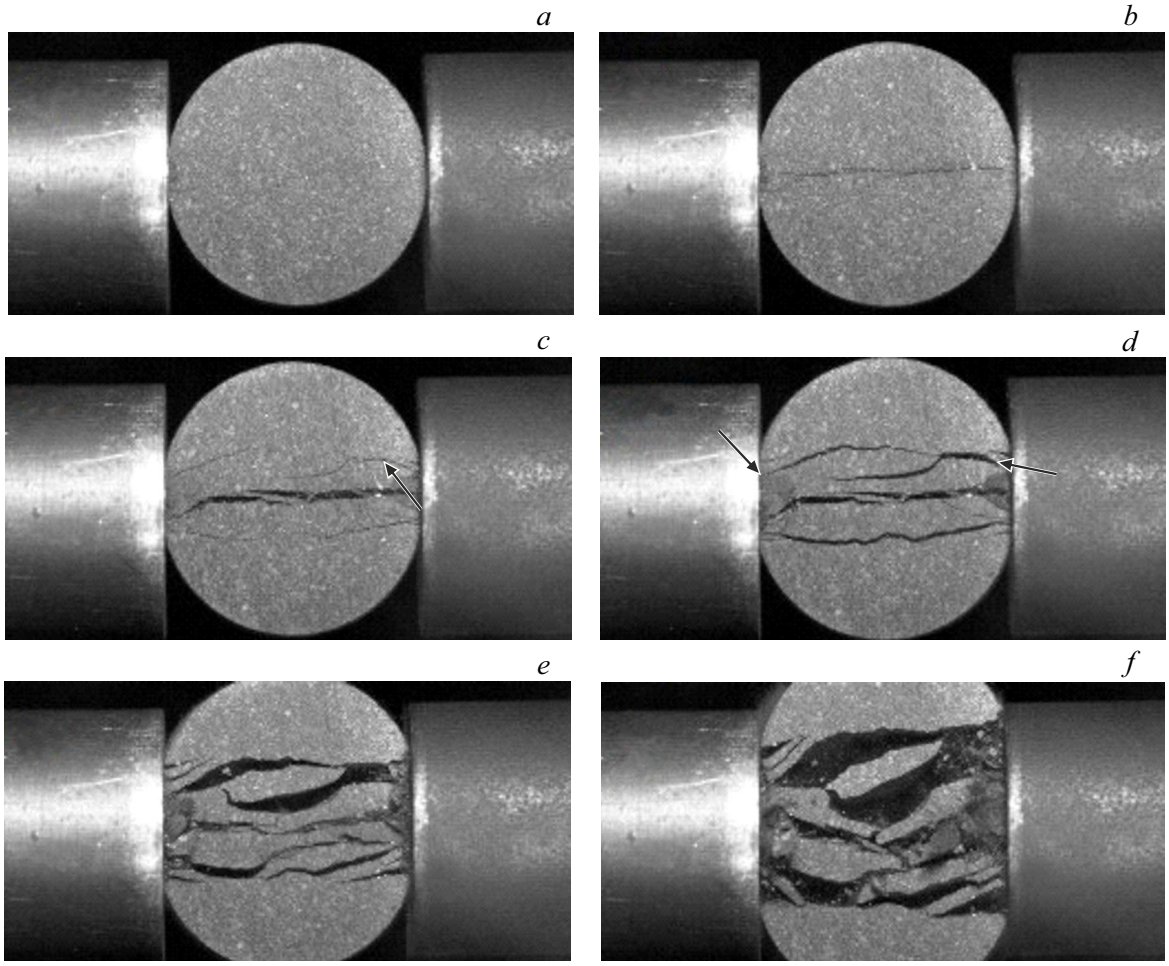

Figure 5. Process of specimen destruction at an impact velocity of 9.37 m/s (arrows indicate the regions of severe deformation (dark areas)).

frames is $\sim 7\,\mu$s, its velocity determined based on the crack half-length is ~ 1500 m/s.

Thus, the SG crack velocity under shock loads falls within the $(0.2-0.25)c_l$ range (c_l is the speed of sound in the bar, which is $c_l = 6045-7845$ m/s in the present case); i.e., it is approximately two times lower than the maximum (according to certain authors) crack velocity of $0.38c_l$ [13]. If we set the Poisson's ratio for SG−P 0.5P to $\nu = 0.25$, the transverse speed of sound and the Rayleigh wave velocity are $c_t = 3825-4960$ m/s and $c_R = 0.919c_t = 3515-4560$ m/s, respectively. It follows that the crack velocity determined in the present study falls within the range of $0.33-0.43c_R$. Thus, the resulting crack velocity value (at which crack branching occurs) agrees closely with the data reported in [12].

The obtained results also provide an opportunity to estimate roughly the fracture toughness (critical stress intensity factor KIC) of silicified graphite SG−P 0.5P under shock loading. Ratio $K_{IC} = \sigma_\infty\sqrt{\pi l}$ (σ_∞ is the maximum splitting stress and l is the crack half-length) [14] yields the following estimates: $K_{IC} \approx 17-18\,\text{MPa}\cdot\text{m}^{1/2}$ at an impact velocity of 9.5 m/s and $\approx 18-20\,\text{MPa}\cdot\text{m}^{1/2}$ at ~ 15.5 m/s. Note that more accurate formulae for determining K_{IC} under shock loading may be found in [15]. Unlike the above formula, they contain normalized stress intensity factor $F_1(c_1 t/l)$, which depends on the geometry of a specimen and is presented in graphical form. Unfortunately, we failed to find a suitable formula for our specimen, but it may be noted that the difference between the above K_{IC} values and the ones calculated by a more accurate formula are unlikely to exceed 20−30%.

It is also worth noting that although the values of K_{IC} obtained under shock loading of SG−P 0.5P are rough estimates in nature, they are more than 3.5 times higher than the static values of K_{IC} for thermally expanded graphite [16] and 3 times higher than K_{IC} for aluminum oxide ceramics [17].

2.2. Results of experiments on compression of specimens

The results of experiments are presented in Table 3 and Fig. 7. The loading diagrams are shown in Fig. 8.

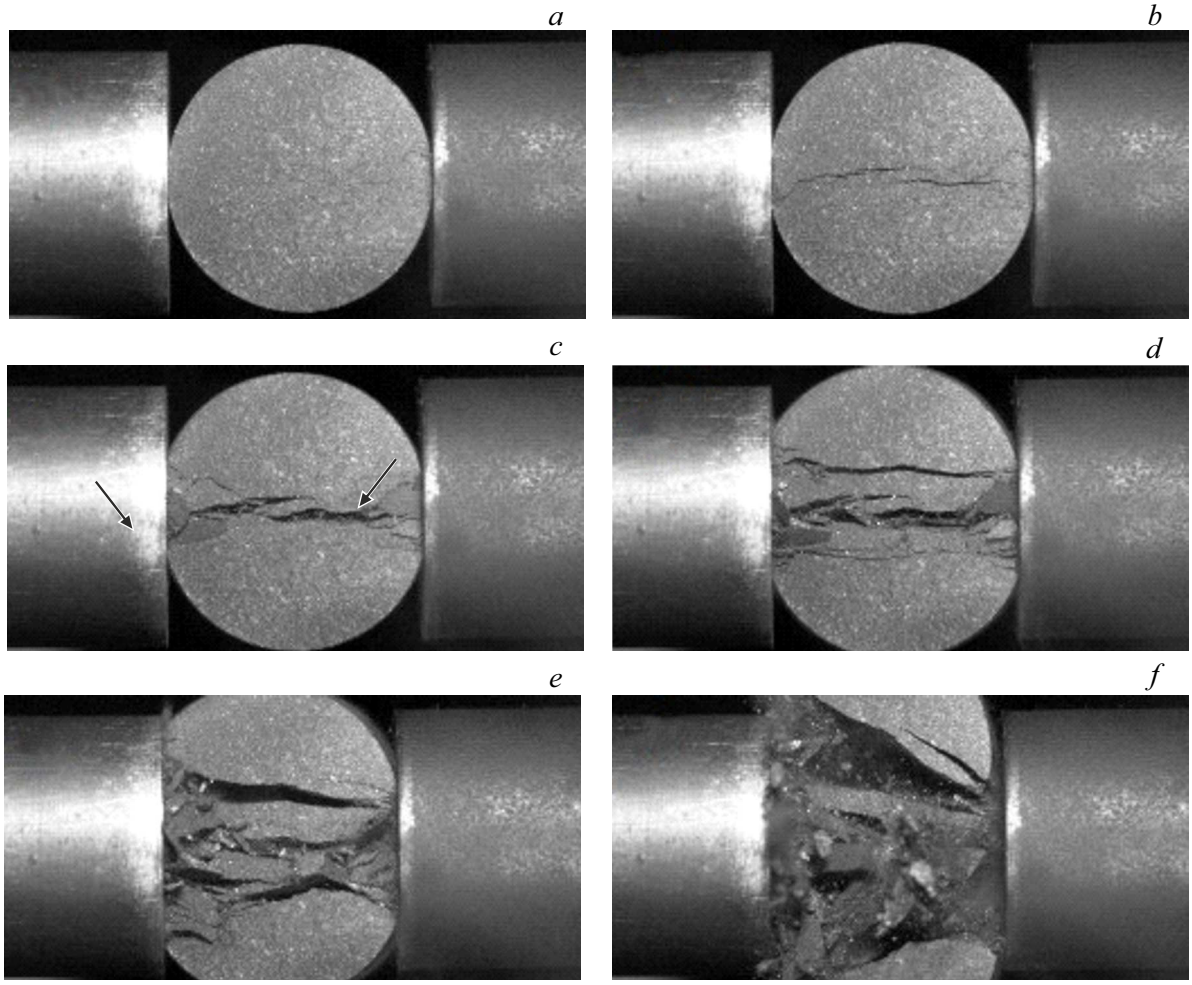

Figure 6. Process of specimen destruction at an impact velocity of 20.69 m/s (arrows denote the regions of severe deformation (dark areas); points indicate the availability of frames shot before and after the given one).

The obtained results demonstrate that the dynamic ultimate compressive strength is 2–4 times higher than the corresponding static strength. As with splitting in the tested range of deformation rates, the dependence of the dynamic ultimate compressive strength on the specified rate is virtually linear (Fig. 7).

2.3. Analysis of loading diagrams under tension and compression

The following aspect stands out when one examines the loading diagrams under splitting (tension). The slopes of the loading curve are equal (α_0) at all impact velocities within the elastic segment; therefore, Young's moduli E are also equal, since E is a linear function of $\mathrm{tg}\,\alpha_0$ [18].

The compression diagrams reveal the following. At deformation rate $\dot{\varepsilon} \approx 700\,\mathrm{s}^{-1}$, $\mathrm{tg}\,\alpha_0$ matches the corresponding tangents for tension, but the tangents at deformation rates of 1800 and $2600\,\mathrm{s}^{-1}$ are equal to each other and differ from the tangent at $700\,\mathrm{s}^{-1}$.

Table 3. Results of dynamic compression tests

Test code	Deformation rate, s^{-1}	Ultimate strength, MPa
c718-01	841	333
c718-02	677	350
c718-03	667	348
Average values	728 ± 98	344 ± 9
c718-04	1816	366
c718-05	1776	395
c718-06	1776	416
Average values	1789 ± 19	392 ± 25
c718-08	2654	447
c718-09	2722	458
c718-10	2552	444
Average values	2643 ± 85	450 ± 7

A comparison of Figs. 5 and 6 with the time interval between frames taken into account suggests that the deformation rate in this case is ~ 400–$600\,\mathrm{s}^{-1}$; in other

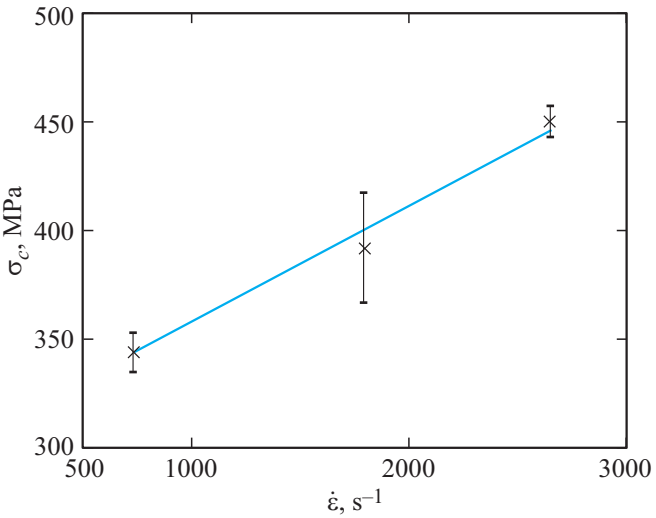

Figure 7. Dependence of the dynamic ultimate compressive strength on the deformation rate.

words, it is close to (virtually the same as) rate $\dot{\varepsilon} \approx 700\,s^{-1}$. Thus, it may be assumed that the Young's moduli under tension/compression and elevated loading rates match if the deformation rates are equal and do not exceed $10^3\,s^{-1}$. At deformation rate $\dot{\varepsilon} > 10^3\,s^{-1}$, the Young's modulus under compression increases, but further experimental studies are needed to verify its equality to the Young's modulus under tension.

It is surprising that the Young's modulus varies (increases) with increasing deformation rate. It is known that the Young's modulus, which is a physical constant of a material, may change under ultrahigh rates of loading (by nanosecond laser or electron pulses) when the accompanying processes become substantially non-equilibrium, non-stationary, and non-local (see [19] and references therein; all the reported data correspond to aluminum). The conditions in the present case are different, but one possible cause may still be suggested: it is the porosity and compositional heterogeneity of SG−P 0.5P (Table 1). If the material were homogeneous, the dependence of Young's modulus E on porosity ν would take the form [20]

$$E = E_1(1-\eta)^m, \tag{5}$$

where E_1 is the Young's modulus of a porous body matrix and $m = 2-4$ is an index that depends on the porosity structure; i.e., nothing indicates a dependence of E on the deformation rate. Whatever the case may be, additional research is needed to interpret the obtained result (Young's modulus variation).

Conclusion

Experimental studies of the mechanical properties of SG within the range of deformation rates $(k \cdot 10^2 - n \cdot 10^3)\,s^{-1}$ both under tension and compression revealed the following:

(1) the dynamic ultimate strength is 2−4 times higher than the static one;

(2) the critical stress intensity factor under dynamic loading is 3 times higher than the corresponding factor for aluminum oxide ceramics under static loading;

(3) the crack propagation velocity under shock loading of SG is close to the limiting value at which the transition from rectilinear propagation of a crack to its branching is observed.

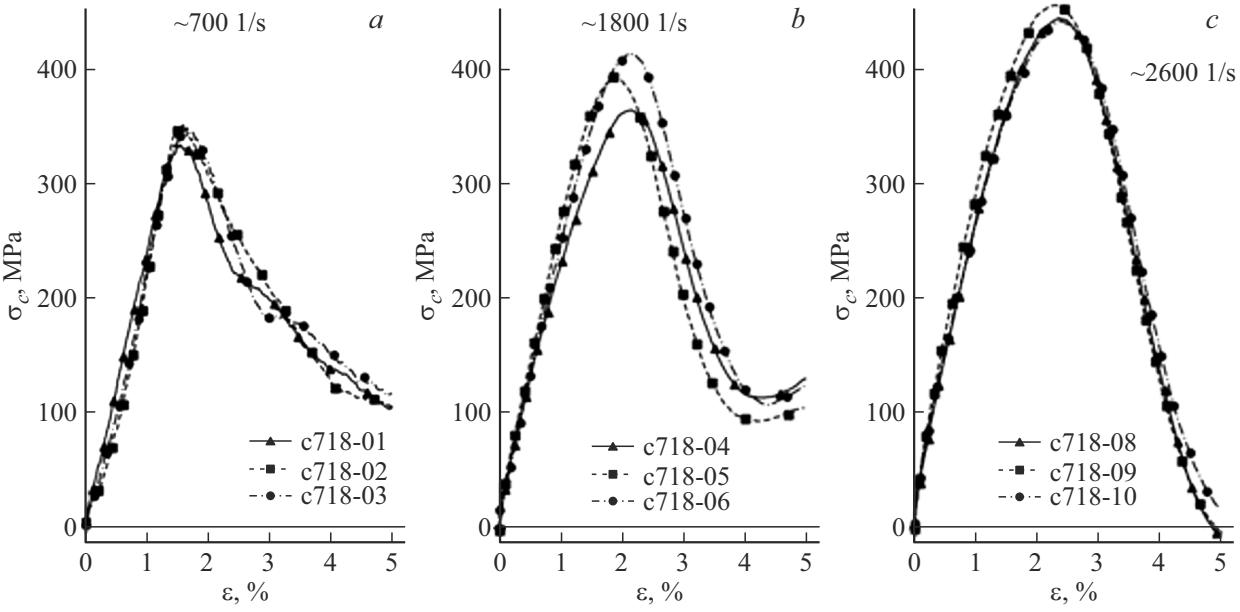

Figure 8. Loading diagrams for specimens under compression.

Conflict of interest

The authors declare that they have no conflict of interest.

References

[1] O.Yu. Sorokin, I.A. Bubnenkov, Yu.I. Koshelev, T.V. Orekhov. Izv. Vyssh. Uchebn. Zaved., Khim. Khim. Tekhnol., **55** (6), 12 (2012) (in Russian).

[2] S.L. Shikunov, V.N. Kurlov. Tech. Phys., **62** (12), 1869 (2017). DOI: 10.21883/JTF.2017.12.45212.2291

[3] B.A. Kalin, P.A. Platnov, Yu.V. Tuzov, I.I. Chernov, Ya.I. Shtrombakh. *Konstruktsionnye materialy yadernoi tekhniki* (NIYaU MIFI, M., 2012) (in Russian).

[4] O. Dezellus, S. Jacques, F. Hodaj, N. Eustathopoulos. J. Mater. Sci., **40** (9–10), 2307 (2005). DOI: 10.1007/S10853-005-1950

[5] *Carbon Products. Methods of Determination for Compressive, Bend, Tensile Strengths (Diametral Compression)*: GOST 23775–79 (Izd. Standartov, M., 2001) (in Russian).

[6] A.M. Neville. *Properties of Concrete* (Pitman Publishing, London, 1973)

[7] T. Rodriguez, C. Navarro, V. Sanchez-Galvez. J. Physique, **IV**, 101 (1994). DOI: 10.1051/jp4:1994815

[8] A.M. Bragov, A.K. Lomunov. *Ispol'zovanie metoda Kol'skogo dlya issledovaniya protsessov vysokoskorostnogo deformirovaniya materialov razlichnoi fizicheskoi prirody* (Izd. Nizhegorod. Gos. Univ., Nizhnii Novgorod, 2017) (in Russian).

[9] K. Ravi-Chandar. Inter. J. Fracture, **90**, 83 (1998). 8r

[10] J.-B. Leblond, J. Frelat. Intern. J. Solids Structure, **37**, 1595 (2000).

[11] V.M. Kornev. Fiz. Mezomekh., **6** (5), 37 (2003) (in Russian).

[12] K. Ravi-Chandar, W.G. Knauss. Intern. J. Fracture, **26**, 65 (1982).

[13] D. Broek. *Elementary Engineering Fracture Mechanics* (Noordhoff International Publishing, Leyden, 1974)

[14] V.I. Vladimirov. *Fizicheskaya priroda razrusheniya materialov* (Metallurgiya, M., 1984) (in Russian).

[15] *Stress Intensity Factors Handbook*, Ed. by Y. Murakami (Pergamon Press, 1987), Vol. 2.

[16] L.R. Vishnyakov, B.N. Sinaiskii, E.P. Kosygin, E.Yu. Chizhan'kov, V.T. Varchenko. Nov. Mater. Tekhnol. Metall. Mashinostr., **2**, 41 (2006) (in Russian).

[17] G.A. Gogotsi. Strength Mater., **38** (3), 261 (2006).

[18] N.A. Shaposhnikov. *Mekhanicheskie ispytaniya metallov* (Mashgiz, M.-L., 1951) (in Russian).

[19] G.G. Savenkov, V.A. Morozov, A.V. Kuznetsov, B.K. Barakhtin, A.A. Lukin. Deform. Razrushenie Mater., 4, 31 (2016) (in Russian).

[20] V.S. Zarubin, I.Yu. Savel'eva, E.S. Sergeeva. Inzh. Zh.: Nauka Innovatsii, 12, 1 (2017) (in Russian). DOI: 10.18698/2308-6033-2017-12-1709

Translated by D.Safin